Letters

Highly Efficient 800-to-48-V *LLC*-DCX With Matrix Transformer Using Side Leg Windings

Yihui Zhang, *Student Member, IEEE*, Hao Feng, *Member, IEEE*, and Li Ran, *Fellow, IEEE*

***Abstract*—Adding side legs to a matrix transformer to achieve magnetic flux diversion and improve core utilization can effectively reduce core losses. The current approach of optimizing air gap is challenging in manufacturing and adjusting parameters. This letter proposes a side leg winding solution to naturally divert flux and achieve flux averaging among all the legs, where an off-the-shelf core can be applied to facilitate fabrication. In addition, the side leg windings are connected in series to enable adoption of low-voltage devices with better equivalent figure of merit. It helps improve efficiency in a high-voltage application. Finally, the proposed structure is verified on an 800-to-48-V 3-kW *LLC*-DCX prototype, achieving a peak efficiency of 98.5% and a power density of 650 W/in^3.**

***Index Terms*—High efficiency, *LLC*-DCX, magnetic flux shunting, matrix transformer, side leg windings.**

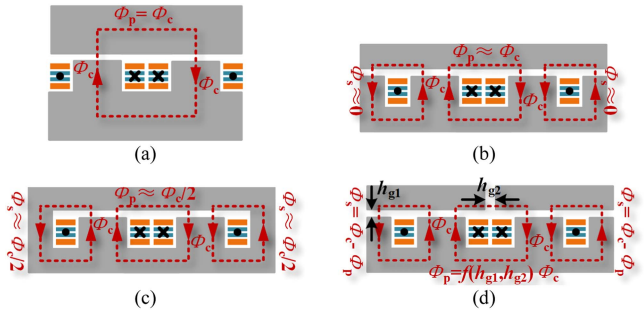

Fig. 1. Different MT. (a) Conventional MT. (b) MT with side legs and uniform air gaps. (c) MT with side legs and air gaps in the plate. (d) MT with side legs and no side leg air gaps.

I. Introduction

MATRIX transformers (MTs) are widely used due to their advantages of low profile, modularity, simplicity in manufacturing, and power density [1], [2]. They can be configured to simultaneously reduce the magnetic flux stress on specific core legs and the current stress on the windings, achieving a high efficiency.

Similar to U-core transformers, magnetic plates with the same thickness as the center legs are needed to ensure uniform flux density in the overall MT, as shown in Fig. 1(a). This is not conducive to a flat design and also increases eddy losses in the core [3]. For commercial cores, using an E-core instead of a U-core allows the center leg flux to be split to two side legs, reducing the thickness of the plates, enabling a more compact design and reduced eddy losses.

In the structure with uniform air gaps, as depicted in Fig. 1(b), the opposite flux produced by the center leg windings in the MT cancels out in the side legs, leading to low utilization of the side legs and ineffective reduction of core losses. In this case, most of the center leg flux still passes through the plate between the center legs, and reducing the thickness of the plate indiscriminately would result in excessive core losses. In other words, adding side legs cannot automatically achieve flux shunting. As shown in Fig. 1(c), the literature [4] eliminates the air gaps at the side legs. The side legs are designed with shorter magnetic paths and higher permeability. The reluctance of the side legs is close to that of the plates between the center and side legs, resulting in better flux distribution. In such a design, parameters, such as magnetizing inductance, are highly sensitive to air gap widths. It requires ultrahigh precision for the nonuniform air gap in all the legs. Once the structure is settled, the air gap in the center leg can no longer be adjusted. It brings major difficulty in mass manufacturing and fabricating the air gap. As depicted in Fig. 1(d), the literature [5] introduces additional air gap between the center legs in the MT, which hinder the flow of reverse flux into the side legs. By controlling the width of additional air gap in the plates, the flux density in the side legs is kept close to that in the center legs, thereby improving the overall utilization of the core. However, the degree of flux uniformity is sensitive to air gap widths. Poorly designed additional air gap widths can lead to higher core losses. Besides, it is necessary to adjust both the original uniform air gap width h_{g1} and the additional air gap width h_{g2} simultaneously to achieve the desired magnetizing inductance and ensure flux averaging. The additional variable increases the design complexity. In general,

Received 5 July 2024; revised 24 August 2024; accepted 17 September 2024. Date of publication 24 September 2024; date of current version 12 December 2024. This work was supported by the National Natural Science Foundation of China under Grant 52107179. *(Corresponding author: Hao Feng.)*

Yihui Zhang and Hao Feng are with the State Key Laboratory of Power Transmission Equipment Technology, School of Electrical Engineering, Chongqing University, Chongqing 400044, China (e-mail: yhzhang21@cqu.edu.cn; hfeng6@cqu.edu.cn).

Li Ran is with the State Key Laboratory of Power Transmission Equipment Technology, Chongqing University, Chongqing 400044, China, and also with the School of Engineering, University of Warwick, CV4 7AL Coventry, U.K. (e-mail: l.ran@warwick.ac.uk).

Color versions of one or more figures in this article are available at https://doi.org/10.1109/TPEL.2024.3467105.

Digital Object Identifier 10.1109/TPEL.2024.3467105

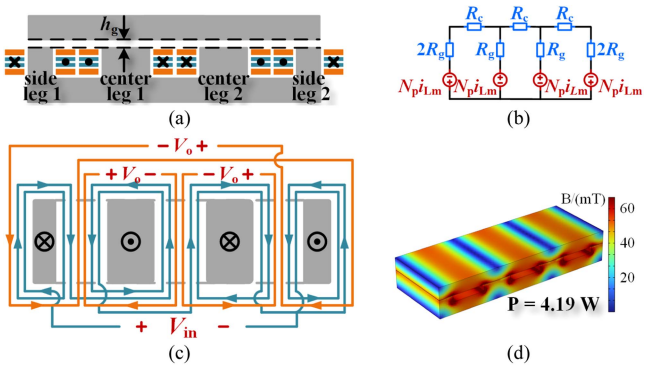

Fig. 2. Exemplary case: three-output MT with side leg windings. (a) Cross-sectional diagram. (b) Equivalent magnetic circuit. (c) Series–parallel structure. (d) Flux density simulation.

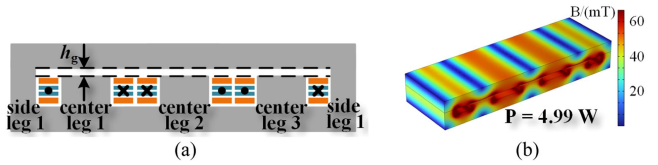

Fig. 3. Exemplary case: three-output MT without side leg windings. (a) Cross-sectional diagram. (b) Flux density simulation.

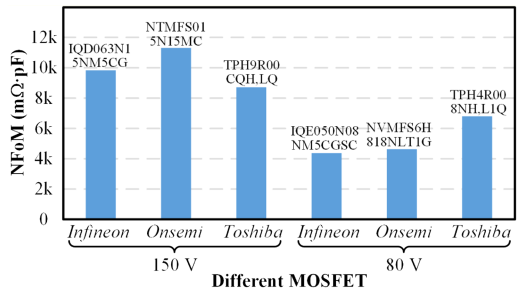

Fig. 4. NFoM of different MOSFETs.

the current approaches to altering the air gap structure either require dedicated manufacturing precision in the air gap widths or are hard to fabricate.

This letter proposes an MT with side leg windings, which achieves flux shunting without changing the air gap structure. It significantly reduces the difficulty of fabrication while preserving the flexibility to adjust air gap. The MT's efficiency and power density are not compromised. The proposed structure is verified on an 800-to-48-V 3-kW *LLC*-DCX prototype, achieving a peak efficiency of 98.5% and a power density of 650 W/in^3.

II. Operating Principle

Adding side leg windings to the MT shown in Fig. 1(b) results in the MT, as shown in Fig. 2. Fig. 2(b) presents the equivalent magnetic circuit. The core's magnetic reluctance can be approximated as negligible because the reluctance of the air gap is much larger. Given that the cross-sectional area of side legs is only half that of the center leg, its magnetic reluctance is approximately double. The series-connected primary windings have the same number of turns and magnetizing current at each leg, producing a magnetic motive force (MMF) with the same amplitude in the magnetic circuit. According to Kirchhoff's law, the flux in the side legs is half of that in the center legs, achieving active flux shunting and uniform flux density distribution within the core, which is validated in Fig. 2(d). Correspondingly, the output voltage of the secondary windings in the side legs is half that of the center legs. The secondary windings in the two side legs are connected in series and then paralleled with the secondary windings of center leg, forming three parallel output units, shown in Fig. 2(c). Functionally, the two-center-leg unit MT with side leg windings is equivalent to the conventional three-center-leg unit MT shown in Fig. 3. Comparatively, the side leg winding structure reduces the core volume and core losses by about 15% (In this simulation case, winding width is half the center leg width). The series current on the primary side ensures current balance among the parallel units on the secondary side, while the symmetrical side leg structure ensures equal voltage distribution across the side leg MOSFETs.

The side leg winding structure not only changes the MT itself but also replaces the high-voltage MOSFETs at the center leg with two series-connected low-voltage MOSFETs at the side leg in the rectifier output. Studies have shown that the equivalent figure of merit [new figure of merit (NFoM), $R_{\mathrm{dson}} \times C_{\mathrm{oss\_tr}}$] of multiple MOSFETs in series is the same as that of a single MOSFET [8], [9], and the NFoM of low-voltage Si devices is much better than that of high-voltage ones, as shown in Fig. 4. Therefore, using the side leg windings also implies a higher efficiency on the rectifier.

For the 800-to-48-V 3-kW series half-bridge (SHB) *LLC*-DCX design, the transformer is expected to provide an 8:1 turns ratio, enabling the *LLC* to operate near the resonant frequency for higher efficiency. The secondary side uses a center-tapped rectifier. To integrate synchronous rectification (SR) MOSFETs on the secondary side and reduce terminal losses, the printed circuit board (PCB) outer layer is used as the secondary winding with the number of secondary turns $N_s = 1$. Hence, the relationship between the primary winding turns N_p and the number of parallel output units n is

$$nN_p = 8. \tag{1}$$

The flux density in the *LLC* transformer is a function of output voltage V_o and is expressed as

$$B_m = \frac{V_o N_p}{4N_s f_s A_e} \tag{2}$$

where f_s is the working frequency, and A_e is the core leg cross-sectional area.

According to the Steinmetz formula [6], the core loss density is expressed as follows:

$$P_v = C_m f_s^{\alpha} B_m^{\beta}. \tag{3}$$

In the *LLC*-DCX, the magnetizing inductance only needs to provide the magnetizing current to achieve zero-voltage switching (ZVS) and does not need to perform voltage regulation. Therefore, the magnetizing current is usually small, and the Dowell 1-D model shown in (4) can effectively predict the ac

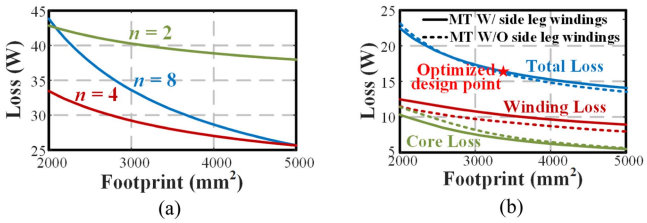

Fig. 5. Minimum loss versus footprint. (a) Sum of transformer losses and SR losses under different n. (b) Transformer losses when $n = 4$.

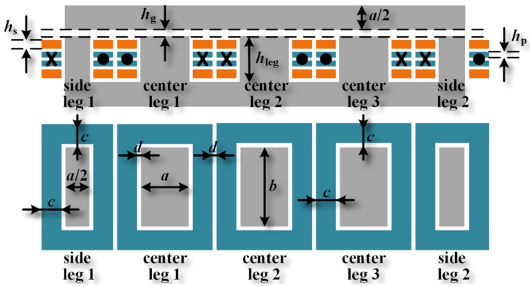

Fig. 6. Four-parallel-output MT with side leg windings and its dimensions.

resistance [7]

$$\frac{R_{\text{ac}}}{R_{\text{dc}}} = \frac{\varepsilon}{2}\left[\frac{\sinh\varepsilon + \sin\varepsilon}{\cosh\varepsilon - \cos\varepsilon} + (2m-1)^2\frac{\sinh\varepsilon - \sin\varepsilon}{\cosh\varepsilon + \cos\varepsilon}\right] \quad (4)$$

where ε is the ratio of winding thickness h to skin depth δ, and m is the number of layers in a winding porting. Using this model, the appropriate primary winding thickness h_p is 2 oz, and the secondary winding thickness h_s is 3 oz at an operating frequency of 700 kHz.

The number of SR MOSFETs is also correlated with the number of parallel output units n. When the *LLC*-DCX operates near the resonant frequency, the MOSFET losses are predominantly channel conduction losses under SR control in *LLC*, and it can be approximately calculated as

$$P_{\text{SRs}} = ((n-1)R_{\text{dson\_}c} + 2R_{\text{dson\_}s})\left(\frac{\pi P_o}{2\sqrt{2}nV_o}\right)^2. \quad (5)$$

Using the aforementioned loss model, the losses of the MT for different dimensions and numbers of output units n can be obtained. Fig. 5(a) shows the minimum loss versus footprint under different n. It is found that with four parallel output units, the MT with side leg windings, as shown in Fig. 6, can achieve the highest efficiency. Using this MT, an *LLC* converter shown in Fig. 7 is constructed to achieve high-current output at low voltage.

At the same optimization point, the magnetic flux density distribution shown in Fig. 8 was obtained. It was observed that in Fig. 8(b), more magnetic flux flows between the center columns, with less flux flowing between the center and side columns, which is also reflected in Fig. 3(b). This occurs because the magnetic flux in the side and center columns is inversely proportional to the magnetic reluctance between the side columns and the magnetic reluctance of the core between the center columns

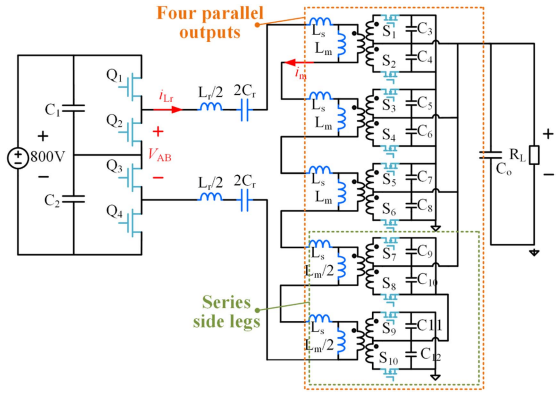

Fig. 7. *LLC*-DCX based on the MT with side leg windings.

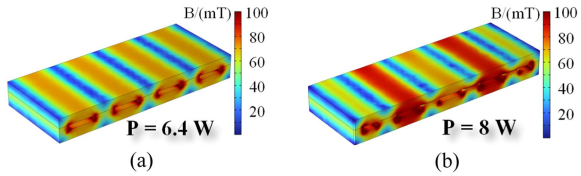

Fig. 8. Flux density simulation. (a) MT with side leg windings. (b) MT without side leg windings.

TABLE I
MT OPTIMIZED PARAMETERS

Parameter	Values
Center leg width a	8 mm
Center leg length b	31 mm
PCB winding width c	4.2 mm
Inner layer copper thickness h_{p}	2 oz
Outer layer copper thickness h_{s}	3 oz
Primary winding turns N_{p}	2
Secondary winding turns N_{s}	1
Core material	3F36

[4]. This unevenly distributed flux results in higher core losses in the design without side columns than initially expected. As comparison, the proposed side leg winding solution features a uniform flux and thereby lowers core loss.

The MT with side leg windings reduces the number of center legs, thus reducing core losses. However, the introduction of side leg windings brings additional copper losses. Therefore, optimizing this MT involves a tradeoff between core losses and copper losses. Fig. 5(b) compares the efficiency of a four-output MT with and without side leg windings. The reduced core losses compensate for extra winding losses so that the proposed design does not sacrifice efficiency or power density. In the meantime, the transformer applies regular E-core with uniform air gap, so the normal air gap structure is preserved. Moreover, the flux shunting effect does not depend on the air gap, so that it can be tuned purely for the magnetizing inductance. From the Pareto-front curve, the optimized parameters are given in Table I.

To further reduce core losses without decreasing power density, the core structure can be improved, as shown in Fig. 9. The SRs and output capacitors are placed on the one side of the MT, while the other three sides have windings around the core. The plate extends to align with three edges, further lowering the

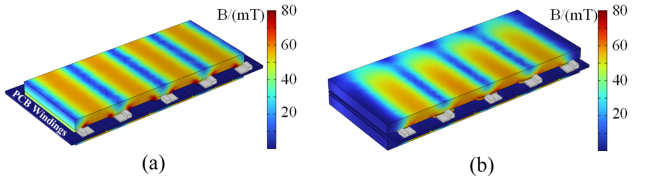

Fig. 9. Improvement of the proposed structure to further reduce the core loss. (a) Initial structure. (b) Structure that extends plates to the three edges without components.

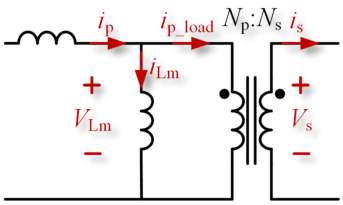

Fig. 10. Transformer model.

flux density in core and reducing core losses. Simulation results indicate that core losses are decreased by approximately 15%.

Although the impedances of the side leg windings and SRs differ from those of the center leg, this does not result in significant current-sharing issues. On the one hand, the impedance differences caused by the windings and SRs are small compared with the load impedance. On the other hand, there is a current-sharing negative feedback mechanism in planar transformers. In the *LLC* converter, the currents shown in Fig. 10 are nearly in phase. Under this premise, if the RMS value of the secondary winding current i_s in one magnetic column unit increases, the RMS value of i_{p_load} also increases. Since the primary windings are connected in series, the current i_p in each magnetic column unit remains equal, which leads to a decrease in the RMS value of the magnetizing current i_{Lm}. This results in a reduction in the voltage across the magnetizing inductance V_{Lm}, which, in turn, reduces the transformer's secondary output voltage V_s. Consequently, the secondary winding current decreases, maintaining balanced current distribution across the transformer.

In this structure, the secondary winding on the side leg generates an MMF opposite to that of the primary winding, reducing the MT leakage inductance, making it suitable for *LLC*-DCX design. If the secondary winding on the side leg is removed, leaving only the primary winding to achieve flux shunting, a leakage inductance is then produced to fulfill the voltage regulation requirement. Therefore, removing the secondary's side leg winding is a promising magnetic integration solution for resonant inductors, which is not further discussed in this letter.

III. Experimental Verification

The design concept is verified on a 3-kW 800-to-48-V *LLC*-DCX, as shown in Fig. 11. The key parameters of the prototype are shown in Table II. Q_1–Q_4 use 650-V GaN devices, and the switching frequency of the converter is 700 kHz. The high switching frequency helps to reduce the MT size and further improve the power density of the converter. The dimensions of

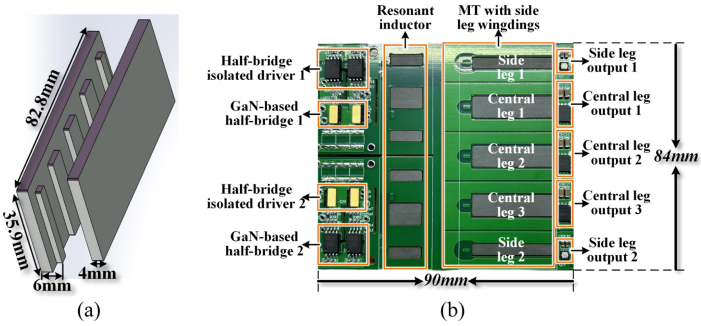

Fig. 11. *LLC* based on MT with side leg wingdings. (a) MT with side leg wingdings. (b) *LLC* converter prototype.

TABLE II
LLC Prototype Parameters

Parameter	Values
Primary GaN device	GS66508T
Center leg SR MOSFET	IQD063N15NM5CG
Side leg MOSFET	IQE050N08NM5CGSC
Magnetizing inductance	40 µH
Resonant inductance	1.1 µH
Input voltage	800 V
Output voltage	48 V
Output power	3 kW
Resonant frequency	700 kHz

TABLE III
Comparison of DC–DC Converters With Voltage Levels of 800 V and Above

Reference	[10]	[11]	[12]	This work
Power rating	5 kW	1.2 kW	3 kW	3 kW
Input voltage	800 V	800 V	1000 V	800 V
Output voltage	48 V	14 V	32 V	48 V
Peak efficiency	97.8%	93.4%	96.4%	98.5%
Full-load efficiency	97.4%	91.6%	96.2%	98%
Switching frequency	100 kHz	700 kHz	1 MHz	700 kHz
Power density	81.9 W/in^3	167.1 W/in^3	107 W/in^3	650 W/in^3

the prototype are 90 mm (length) × 84 mm (width) × 10 mm (height). The power density can reach 650 W/in^3.

Table III compares the dc–dc converter at voltage level of around 800 V. It turns out that the efficiency and power density of presented work is beyond state of the art.

Fig. 12 shows the key waveforms of the converter operating at full load. It is observed that the voltages across the two-side-leg MOSFETs are almost identical, indicating good series voltage sharing. The side leg SRs operate at half the voltage of the center leg rectifier MOSFETs, enabling a good series–parallel operation. It is also found from Fig. 12(b) that the center leg can achieve good series voltage sharing among the same signal-controlled GaN switches, allowing the 650-V devices to operate under an 800-V bus voltage. Moreover, ZVS can be achieved under full-load conditions.

Figs. 13 and 14 show the operating waveform under light load. They show ZVS over a wide load range securing high efficiency. The side leg voltage balancing also holds at light load.

It is also noted that a split resonant inductor is added to facilitate ZVS of primary devices, which can be easily lost due to high parasitic capacitance of secondary MOS and high

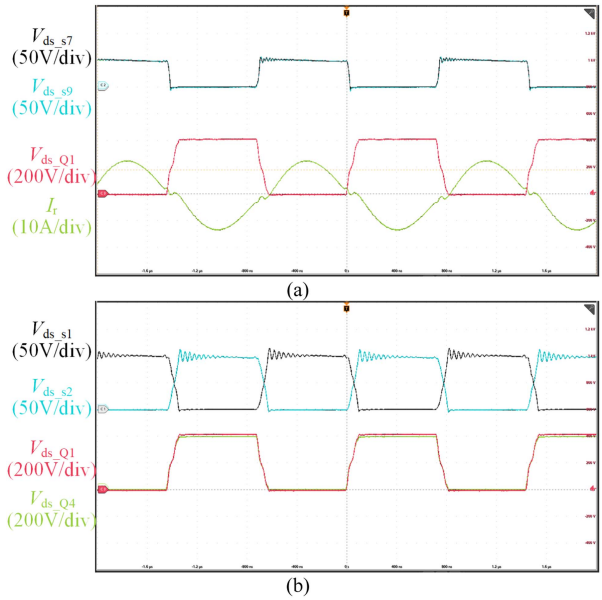

Fig. 12. Full-load operating waveform.

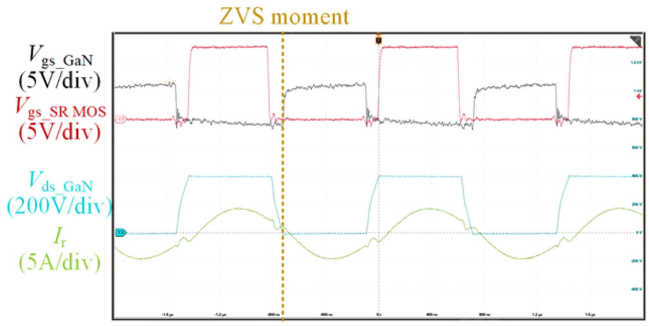

Fig. 13. ZVS waveform under 33% load condition.

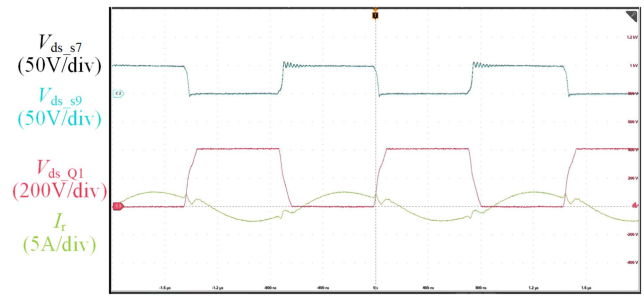

Fig. 14. 20% load operating waveform.

turn's ratio. This is a major difference compared to regular lower voltage DCXs.

The converter efficiency is tested at nominal conditions using high-precision programmable dc supply IT6006D-800-25 and electronic load Chroma 63205A-1200-200. Fig. 15(a) illustrates the efficiency at different power levels, reaching peak efficiency 98.5%. The full-load efficiency reaches 98%, and relatively high average efficiency is also maintained around half-load. The loss analysis of the full load is given in Fig. 15(b). According to the

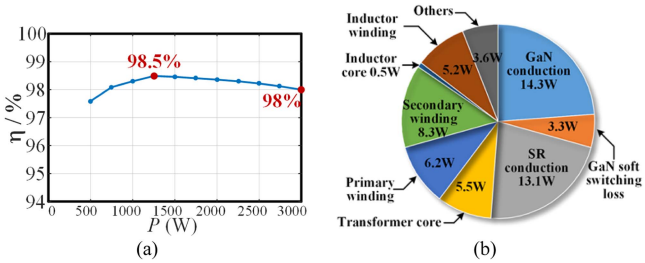

Fig. 15. Efficiency and losses. (a) Tested efficiency. (b) Loss breakdown at full load at 3 kW.

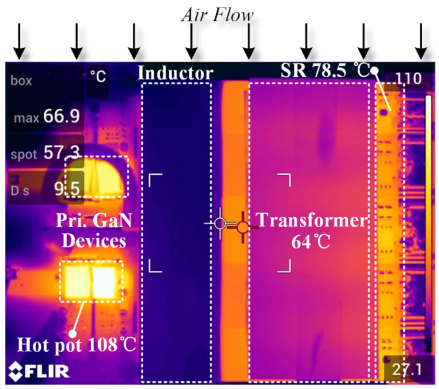

Fig. 16. Thermal performance of the 3-kW *LLC* converter with forced air cooling of 800 LFM.

loss analysis, the total transformer loss is approximately 25 W, which includes core loss and dc and ac copper losses. The total loss on the primary side is approximately 13 W, which includes the turn-OFF switching loss and the conduction loss. Since the *LLC*-DCX operates near the resonant frequency, the SR losses are mainly conduction losses at 16 W. Other losses include PCB trace loss, terminal loss, and input and output capacitor losses.

Fig. 16 shows the thermal performance of the 3-kW prototype under full load and with 800-LFM forced air cooling. The hotspot occurs at 108 °C in the primary SHB. The highest temperature on the secondary side is 78.5 °C. The multiple outputs of the MT split the output power, resulting in a low profile and high surface-to-volume ratio, which improves heat dissipation capability. The balanced flux density over all the legs and plates ensures a uniform loss distribution, and it is reflected by a relatively steady temperature on the plate's upper surface. Generally, the overall temperature is kept reasonable for the MT and SR MOSFETs nearby.

IV. Conclusion

Adding side legs to the MT to achieve magnetic flux diversion and improve core utilization can effectively reduce core losses. However, it requires modifying the air gap structure, and fabricating small and precise air gaps in MTs is often subjected to manufacturing error. This letter proposes an MT structure with side leg windings, which achieves magnetic flux shunting without resorting to complex air gap structures. This approach increases the core utilization, significantly reducing the

manufacturing difficulties, and preserves the flexibility to tune air gap. The series side leg winding also proves to be an ideal solution for high-voltage DCX in automotive applications. The feasibility of the proposed scheme is verified in an 800-to-48-V 3-kW *LLC*-DCX prototype, achieving a peak efficiency of 98.5% and a power density of 650 W/in^3.

REFERENCES

[1] M. Mu and F. C. Lee, "Design and optimization of a 380–12 V high-frequency, high-current LLC converter with GaN devices and planar matrix transformers," *IEEE J. Emerg. Sel. Topics Power Electron.*, vol. 4, no. 3, pp. 854–862, Sep. 2016.

[2] C. Fei, F. C. Lee, and Q. Li, "High-efficiency high-power-density LLC converter with an integrated planar matrix transformer for high-output current applications," *IEEE Trans. Ind. Electron.*, vol. 64, no. 11, pp. 9072–9082, Nov. 2017.

[3] A. Nabih, F. Jin, R. Gadelrab, F. C. Lee, and Q. Li, "Characterization and mitigation of dimensional effects on core loss in high-power high-frequency converters," *IEEE Trans. Power Electron.*, vol. 38, no. 11, pp. 14017–14036, Nov. 2023.

[4] A. Nabih and Q. Li, "Design of 98.8% efficient 400-to-48-V *LLC* converter with optimized matrix transformer and matrix inductor," *IEEE Trans. Power Electron.*, vol. 38, no. 6, pp. 7207–7225, Jun. 2023.

[5] M. K. Ranjram and D. J. Perreault, "Leveraging multi-phase and fractional-turn integrated planar transformers for miniaturization in data center applications," in *Proc. IEEE 21st Workshop Control Model. Power Electron.*, Aalborg, Denmark, 2020, pp. 1–8.

[6] V. C. Valchev and A. Van den Bossche, *Inductors and Transformers for Power Electronics*. New York, NY, USA: Taylor & Francis, 2005.

[7] P. L. Dowell, "Effects of eddy currents in transformer windings," *Proc. Inst. Elect. Eng.*, vol. 113, pp. 1387–1394, 1966.

[8] X. Wu and H. Shi, "High efficiency high density 1 MHz 380–12 V DCX with low FoM devices," *IEEE Trans. Ind. Electron.*, vol. 67, no. 2, pp. 1648–1656, Feb. 2020.

[9] G. Fan, X. Wu, T. Liu, and Y. Xu, "High-efficiency high-density MHz cellular DC/DC converter for on-board charger," *IEEE Trans. Power Electron.*, vol. 37, no. 12, pp. 15666–15677, Dec. 2022.

[10] X. Du, F. Diao, Y. Zhao, K. Uvodich, and N. Miljkovic, "A high-density 5kW 800V to 48VDC/DC converter for vehicle applications," in *Proc. IEEE Energy Convers. Congr. Expo.*, Vancouver, BC, Canada, 2021, pp. 1502–1506.

[11] H. P. Kieu, D. Lee, S. Choi, and S. Kim, "A 700 kHz 800V/14V GaN-based DC-DC converter with optimized integrated transformer for electrical vehicles," in *Proc. IEEE Energy Convers. Congr. Expo.*, Vancouver, BC, Canada, 2021, pp. 5549–5553.

[12] Z. Zhang et al., "1-kV input 1-MHz GaN stacked bridge *LLC* converters," *IEEE Trans. Ind. Electron.*, vol. 67, no. 11, pp. 9227–9237, Nov. 2020.